Carbon 245 (2025) 120747

Contents lists available at ScienceDirect

Carbon

journal homepage: www.elsevier.com/locate/carbon

Single-cell insights into carbon dots interactions with plant cell walls for distinct internalization pathways via surface charge modulation

Luyao Wei [a,b], Binshou Wang [a,b], Shuling Cao [a,b], Hang Tan [c], Tianyi Long [a,b], Chuanfei Bian [a], Liangcai Peng [d,e], Hongliang Wang [a,b], Xu Cheng [a], Wanbin Zhu [a,b,*]

[a] Center of Biomass Engineering/College of Agronomy and Biotechnology, China Agricultural University, Beijing, 100193, China
[b] Sanya Institute of China Agricultural University, Sanya, 572025, China
[c] School of Breeding and Multiplication (Sanya Institute of Breeding and Multiplication), Hainan University, Sanya, 572025, China
[d] Key Laboratory of Fermentation Engineering (Ministry of Education), Hubei Key Laboratory of Industrial Microbiology, Cooperative Innovation Center of Industrial Fermentation (Ministry of Education & Hubei Province), School of Life and Health Sciences, Hubei University of Technology, Wuhan, 430068, China
[e] College of Plant Science & Technology, Huazhong Agricultural University, Wuhan, 430070, China

ARTICLE INFO

Keywords:
Charged carbon dots
Plant cell internalization pathways
Multi-layered plant barriers
Cell wall polymers
Vesicle formation

ABSTRACT

Although nanoparticles have been applied in plant biotechnology, much remains unknown about carbon dots (CDs) uptake and translocation in plant cells. Here, we synthesized glucose-derived CDs (GCDs, +44.3 mV) and lignin-derived CDs (LCDs, −16.2 mV) to investigate charge-dependent interactions with plant cells. Confocal microscopy of protoplasts revealed much more favored uptake of GCDs compared to LCDs following 2 h co-incubation. Leaf exposure experiments confirmed that GCDs exhibit a stronger association with plant cell walls. Meanwhile, FTIR analysis of isolated cell wall fractions indicated that charged-CDs were mainly involved in interactions with hemicelluloses and pectin, including lignin-crosslinked polysaccharides. Furthermore, the GCDs internalization in plant cells caused membrane invagination and vesicle formation for encapsulating GCDs, whereas the LCDs were of dispersed and disorder distribution in cell, as verified by TEM analysis. Hence, this study proposed a hypothetic model about the critical roles of surface charges in modulating CDs interaction with plant cell walls and internalization within cell cytoplasm in plant cells, providing insights into CDs functions in plant growth and development for biomass production.

1. Introduction

Recent advancements in nanotechnology have been driven by tunable physicochemical properties. Within agricultural applications, nanomaterials showed unique capabilities in targeted agrochemical delivery [1,2], genetic engineering optimization [3–5], and real-time crop productivity monitoring [6,7], providing novel pathways for addressing global food security and advancing sustainable agricultural practices. The small dimensions (1–100 nm) and potential to cross biological barriers [8,9] facilitate engineered nanomaterials to interact with living systems in unique ways. Particularly, provide promising opportunities to manipulate plant physiology at cellular and molecular levels [10,11]. However, the behavior and mechanisms of nanoparticles within plant systems remain incompletely understood, particularly their internalization behaviors in plant tissues and cells.

The selectively permeable plasma membrane poses a challenge to nanoparticle entry. Comprehensive studies have underscored mechanism for nanoparticles to enter animal cells [12,13], while plant systems present distinct biological challenges due to the presence of cell wall. Pore size constraints (5–20 nm) and physicochemical heterogeneity of the plant cell wall restrict nanoparticle permeation [14–17]. Nanoparticle size, shape, surface charge, and modifications critically determine penetration efficiency. Electroneutral nanoparticles show limited protoplast entry, whereas ultra-small (<10 nm) nanoparticles with high absolute zeta potential (>40 mV) efficiently enter the cytosol and chloroplasts [18]. There are significant differences in charge dependent interactions between plant and animal systems. Amine-modified polystyrene NPs induce plasma membrane depolarization enhancing animal cell entry, whereas negatively charged nanoceria exhibit higher delivery efficiency into plant cells without membrane depolarization [19,20]. Biological membrane composition within plant cells further modulates interactions. Chloroplast membranes rich in glycerolipids demonstrate

* Corresponding author. Center of Biomass Engineering/College of Agronomy and Biotechnology, China Agricultural University, Beijing, 100193, China.
E-mail address: wanbin@cau.edu.cn (W. Zhu).

https://doi.org/10.1016/j.carbon.2025.120747
Received 14 May 2025; Received in revised form 21 August 2025; Accepted 24 August 2025
Available online 25 August 2025

stronger nanoparticle affinity than phospholipid-dominant protoplast membranes [21]. Current understanding remains constrained by membrane-centric models that neglect plant-specific barrier cascades. Cooperative regulatory mechanisms governing interactions between charged nanoparticles and both cell wall components and membrane remain poorly elucidated. Especially, knowledge on how the charge of nanoparticles affects the morphological change of plant cell membranes, and how the cell wall interacts with charged nanoparticles and regulates their passage across the wall barrier are largely unknown.

Biocompatibility and biotoxicity concerns associated with heavy metal components in conventional nanomaterials (e.g., quantum dots) limit their use in biological systems. In this work, carbon dots (CDs) synthesized from biomass waste streams (lignin, cellulose derivatives) have been employed as an environmentally benign alternative. CDs exhibit multiple advantages including sub-10 nm dimensions, photostability, low cytotoxicity, and facile surface functionalization [22–24]. They have shown unique applications in plants. For instance, CDs alleviate the toxicity of cadmium to crops by adsorbing Cd^{2+} and regulating the expression of related genes [25]. Utilizing renewable bioresource not only minimizes production costs but also enables a closed-loop life cycle through the "synthesis-plant utilization-biomass recycling" framework. In addition, CDs surface engineering allows precise matching charge characteristics of different plant interfaces. This tunability provides an ideal model for studying the interaction between charged nanoparticles and multi-layered plant barriers.

Herein, we systematically investigate charged CDs across two important plant barriers, the cell wall and the cell membrane, by combining multiscale approaches: cell wall-free protoplasts, isolated cell walls, and intact leaves. Confocal microscopy revealed charge-dependent CDs distribution in leaf cells. Interactions between charged CDs and cell walls clarified component-specific translocation roles. In conjunction with biological TEM observations, we demonstrated membrane morphological changes caused by positively charged CDs, and explained CDs traversal mechanisms. This work decouples respective roles of cell wall matrices and membrane in regulating nanoparticle translocate. As demonstration of plant-nanoparticle interactions from multi-interface perspectives, this work establishes a multi-scale analytical framework, which is of great practical significance for advancing development and targeted engineering applications of nanotechnology in plant systems.

2. Materials and methods

2.1. Synthesis of carbon dots

Glucose-derived carbon dots (GCDs) were synthesized by modifying a method reported by Zhao et al. [26]. Briefly, 5 g of glucose was placed in a flask and heated at 150 °C for 30 min, followed by the addition of 5 mL dimethyl diallyl ammonium chloride under continuous stirring (150 °C, 180 min). The cooled brown product was dissolved in DI water, filtered and dialyzed for 48 h. Lignin-derived carbon dots (LCDs) were prepared using alkali lignin (AL) extracted from kraft pulping black liquor via acid precipitation. For LCDs synthesis, 0.5 g AL was mixed with 50 mL DI water, stirred for 20 min, and then heated at 200 °C for 12 h in a hydrothermal reactor [27]. Post-reaction, the mixture was filtered (0.22 μm) and dialyzed (72 h). Both GCDs and LCDs solutions were freeze-dried (−60 °C, 20 Pa) to obtain solid samples for characterization.

2.2. Characterization of carbon dots

Microstructural characterization was conducted on JEOL JEM 2100F TEM (200 kV). Samples were deposited on a Cu/C grid. The functional groups of LCDs and GCDs were detected through an ALPHA II (Bruker, Germany) Fourier transform infrared (FTIR) spectrometer using KBr pellets. The zeta potential of GCDs and LCDs (1 mg/ml) was analyzed by a Malvern Zeta sizer. The photoluminescence (PL) excitation and emission spectra measurements were carried out on a Hitachi F-4700 spectrofluorometer with an Xe lamp as an excitation source.

2.3. Plant growth

Wild-typed *N. benthamiana* seeds were grown in individual 77 mm pots under 16/8 h light/dark photoperiod in artificial greenhouse. Maintain the daytime temperatures at 26 °C and nighttime temperature at 22 °C and 70 % humidity. Infiltration was conducted on the abaxial side of 4 weeks old leaves using a 1 ml needleless syringe.

2.4. Protoplast isolation from Oryza sativa L

Rice protoplasts were isolated from sterile seedlings by slicing shoots into 0.5–1 mm strips and digesting in pre-activated enzyme solution (1.5 % cellulase, 0.75 % macerozyme, 0.6 M mannitol, 10 mM MES, pH 5.7). Tissue-enzymes mixtures were incubated with gentle shaking at 28 °C for 3 h in darkness, then diluted 5-fold with W5 solution (154 mM NaCl, 125 mM $CaCl_2$, 5 mM KCl, 2 mM MES, pH 5.7). Undigested leaf tissue was removed by 70 μm nylon mesh filtration, followed by centrifugation (170×*g*, 7 min) to pellet protoplasts [28]. Freshly isolated protoplasts had been used for internalization studies.

2.5. Extraction of cell wall and conjugation with CDs

Leaf samples were ground in liquid nitrogen and subsequently freeze-dried. 0.3 g of sample was stirred in 5 mL DMSO-water (9:1, v/v) at 150 rpm and 25 °C overnight. Subsequently, the pellets were washed once with DMSO-water and twice with distilled water. The remaining pellets were suspended in 75 % methanol (10 mL, 60 min) and centrifuged (3000×*g*, 5 min). The residues washed with10 mL of 75 % methanol twice, followed by sequential washing steps using 10 mL of each solvent for 20 min: 0.5 % Triton X-100 with 1 M NaCl (once), DI water (twice), 95 % methanol (twice), and acetone (twice). After drying, cell wall material obtained. Cell wall pellets (0.1g) were suspended in 5 mL of $(NH_4)_2C_2O_4$ (0.5 % w/v) for 1 h in a boiling water bath, with vigorous stirring after every 10 min to prevent sedimentation. The supernatants after centrifugation were collected as pectin fraction. The insoluble pellets were further extracted with 5 mL 4 M KOH containing 1.0 mg/mL $NaBH_4$ for 1 h at 25 °C and 150 rpm. Supernatants were pooled as hemicellulose fraction. Pectin and hemicellulose fractions were precipitated with 75 % ethanol, dissolved in water, precipitated again, and then freeze-dried.

100 μl of CDs (0.5 mg/mL) were added into 50 mg cell wall material, pectin and hemicellulose, fully mixed and reacted overnight. The mixture was washed once with deionized water, 95 % methanol, and acetone, then dried. The well-dried samples (2–4 mg) were mixed with KBr at 1:100 (w/w) and pressed into transparent pelletized disc. The spectra were acquired in transmittance mode over 16 scans in the range of 4000 to 400 cm^{-1} region using ALPHA II spectrometer (BRUKER, Germany).

2.6. TEM tracking of CDs in N. Benthamiana leaves

After 12 h infiltration, *N. benthamiana* leaf segments (1 × 3 mm) were fixed with 2.5 % glutaraldehyde under vacuum to evacuate vacuolar air, followed by dehydration with ethanol and acetone and embedding in epoxy resin. For samples used to investigate the internalization pathway, leaves were infiltrated with wortmannin (40 μM) 30 min prior to CDs exposure. The samples were sliced into 100 nm thickness using ultramicrotome and post-fixed with lead citrate and uranyl acetate. The films were transferred onto bare Cu TEM grids for imaging (80 kV).

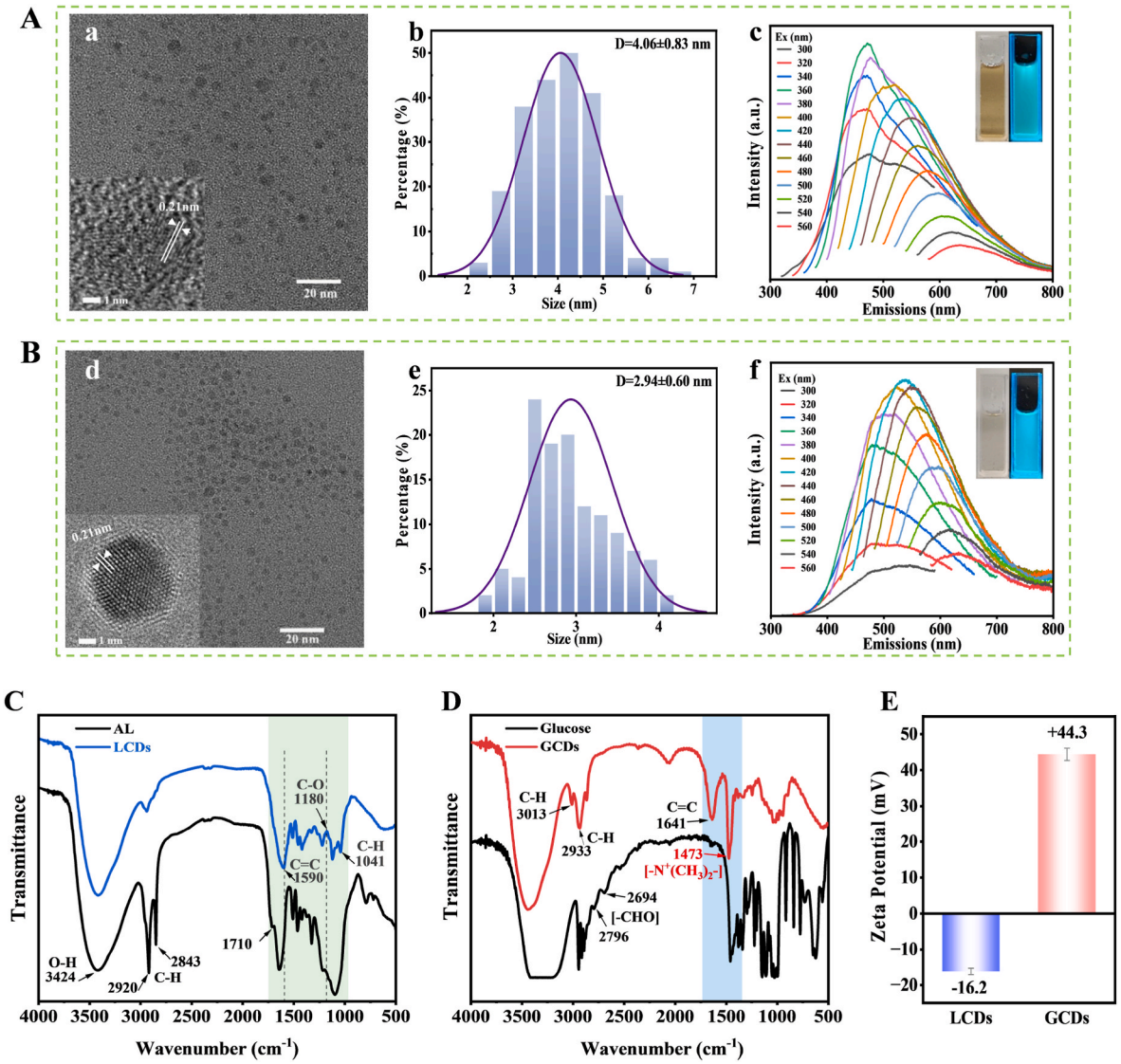

Fig. 1. Morphology, size distribution, fluorescence emission spectra, FTIR spectrum and zeta potential of LCDs, GCDs. (A) and (C): LCDs; (B) and (D): GCDs. Inset of (a, d) are High-resolution TEM images of the CDs. (b, e) are size distribution of the CDs. Inset of (c, f) are photographs of the CDs aqueous solution under sunlight (left) and UV light of 365 nm (right).

3. Results and discussion

3.1. Preparation and characterization of carbon dots

In the process of preparing lignin-based CDs, lignin raw materials need to undergo top-down depolymerization first, and then bottom-up assembly occurs in the reaction system. In the work described here, lignin-based carbon dots (LCDs) were produced from alkali lignin by hydrothermal treatment at 200 °C for 12 h directly [27], and glucose-based carbon dots (GCDs) were synthesized from melting glucose followed by adding dimethyl diallyl ammonium chloride [26].

LCDs and GCDs display well distribution in aqueous solution. TEM images show that the size of LCDs and GCDs range from 2 to 7 nm, and 1.7–4.2 nm, with the average size about 4.06 ± 0.82 nm and 2.94 ± 0.60 nm, respectively (Fig. 1b, e). The pore diameter of plant cell walls and the shape of nanoparticles might be the limitation for the transport of nanoparticles into plant cells [29]. LCDs and GCDs obtained in this study have a nearly spherical shape, with sizes smaller than the pore size exclusion limit range of the cell wall. The more detailed atom resolution structures were detected by High-resolution TEM(HR-TEM). The images reveal well-resolved lattice fringes with inter-crystalline spacings of 0.21 nm for both LCDs and GCDs (inset of Fig. 1a, d), similar to the (100) facets of graphitic carbon, indicating the graphene crystalline structure has relatively few defects [30,31]. Furthermore, hydrodynamic size of the synthesized CDs have been performed by dynamic light scattering (DLS). The number distribution mode in DLS is preferred due to its greater sensitivity to small-size particle signals, thus minimizing the masking effect caused by larger particles. The DLS measurements yielded average hydrodynamic diameters of 27.99 nm for LCDs and 14.97 nm for GCDs, with corresponding polydispersity indices (PDIs) of 0.2097 and 0.2162, respectively (Supplementary Fig. 1). The larger hydrodynamic sizes compared to TEM results are attributed to hydration effects and transient aggregation in aqueous media, consistent with prior reports on highly soluble carbon dots [32,33]. Primary size characterization relied on TEM to reflect core particle dimensions. The as-synthesized LCDs and GCDs aqueous dispersion exhibit clear brown-yellow solutions under daylight and emit bright blue-green fluorescence under irradiation with 365 nm UV light (Fig. 1c, f). Unlike the fluorescence emission of conventional fluorophores such as organic dye, the fluorescence emission of LCDs and GCDs in water depend on the excitation wavelength. The photoluminescence (PL) spectra of LCDs presents a maximum fluorescence emission peak at 540

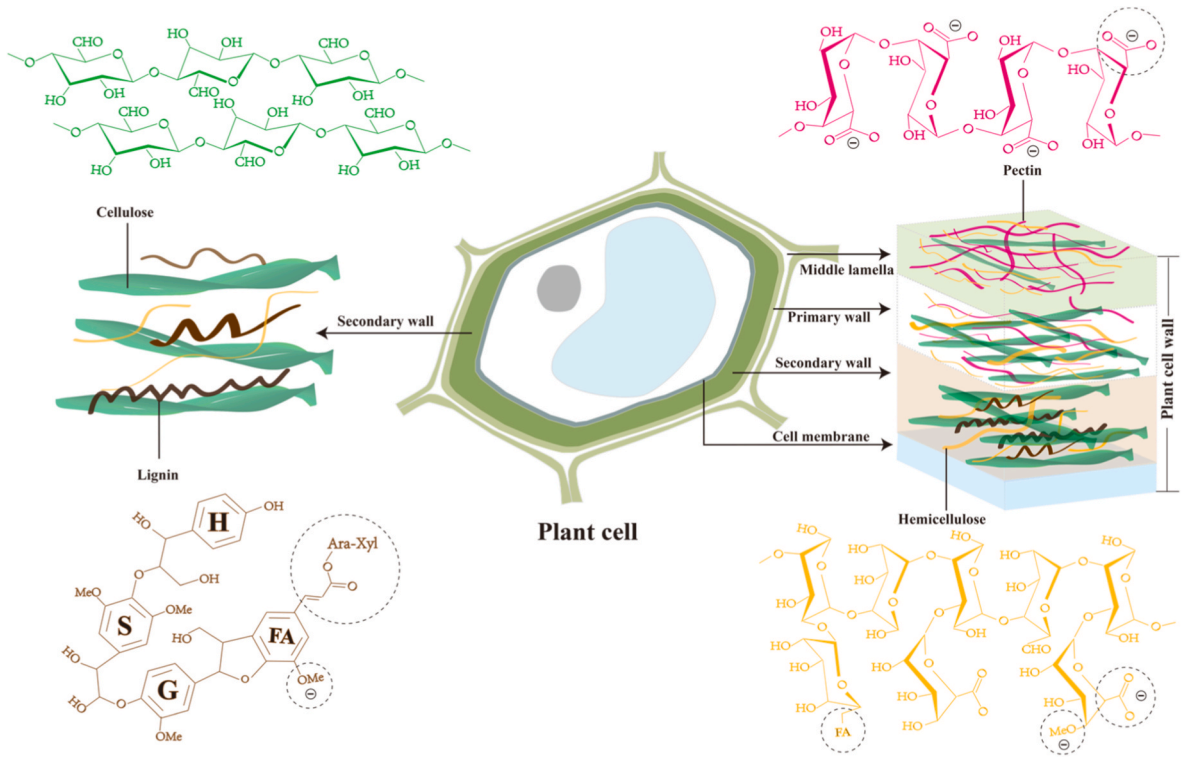

Fig. 2. Schematic illustration of the plant cell and the chemical structures of the main components in plant cell wall. Plant cell wall structure from the inside out are the secondary wall, primary wall, and pectin-rich middle lamella.

nm when excited at 420 nm (Fig. 1c), while emission maximum peak of GCDs is centered at 475 nm with excitation wavelengths of 360 nm (Fig. 1f).

Except for the pore diameters of plant cell walls and the shape mentioned above, another possibility that affects the transportation of nanoparticles in plants might be associated with surface coating/functionalization characteristics. FTIR and zeta potential were carried out to investigate surface characteristics of CDs, as shown in Fig. 1C-E, aiming to better clarify functional groups and charge properties. As depicted in Fig. 1C, the band at 3424 cm^{-1} corresponding to the phenolic O–H and the C–H stretching signals (2920/2843 cm^{-1}) are detected in both AL and LCDs. Except for the groups belonging to AL that are retained, LCDs exhibit enhanced aromatic C═C stretching vibration at 1590 cm^{-1}. Meanwhile, the peak assigned to aromatic ketones/esters groups at 1710 cm^{-1} from AL sharply decreased in LCDs, along with the appearance of the peak at 1180 cm^{-1} associated with C–O and the peak at 1041 cm^{-1} attributed to aromatic C–H. These results demonstrate that LCDs are composed of aromatic skeletons from lignin while developing enhanced π-conjugation through hydrothermal reorganization processes [27,34]. In GCDs, the characteristic absorption peaks ascribing to the aldehyde group (2796 cm^{-1} and 2694 cm^{-1}) in glucose were notably absent, indicating successful cleavage of the aldehyde functionality during the hydrothermal synthesis process (Fig. 1D). Appearance of the peak at 1641 cm^{-1} related to the C═C bond contracting vibration, which might associate with the retaining of C═C bond of dimethyl diallyl ammonium chloride in GCDs, or it might be formed by complex condensation and carbonization of glucose precursor. C═C bond is a typical structure and important component of graphene carbon quantum dots, and it does not exist in glucose. Moreover, the characteristic absorption peak of the C–H bending vibration of $–N^{+}(CH_3)_2$- appeared at 1473 cm^{-1}, which was related to $–N^{+}(CH_3)_2$- in dimethyl diallyl ammonium chloride [26]. These results confirm the successful grafting of quaternary ammonium groups onto GCDs.

Zeta potential analysis shows different charge of LCDs and GCDs owing to surface groups. The zeta potential of LCDs was −16.2 mV might relate to oxygen-containing groups. The cleavage of β-aryl ether linkages in lignin generates phenolic hydroxyl groups, while oxidation-mediated degradation promotes lignin depolymerization accompanied by carboxylic acids formation [35,36]. In contrast, GCDs was +44.3 mV, confirming that GCDs carried abundant positively charged groups (Fig. 1E). The negative charge of LCDs might relate to oxygen-containing functional groups. Properties of nanoparticle surfaces will likely affect botanical interfacial dynamics, thereby modulating nanoparticles translocation in plants [37,38]. Exposure of functionalized AuNPs (amino, hydroxyl, carboxyl) to four herbaceous plants revealed that positively charged AuNPs achieved optimal root absorption, whereas negatively charged counterparts showed superior translocation effective from the roots to other parts [39]. The ionic interactions lead to strong binding between nanoparticles and plant cells. Deprotonation of carboxyl groups on pectin by amine groups resulted in ammonium cations formation [40]. QDs-PEG-COOH interact with the cell wall via hydrogen bonding between carboxyl group and hydroxyl groups [41].

3.2. *Biointerface traversal of charged CDs in intact plant tissues*

The entry of nanoparticles into plant cells can be broadly categorized into three distinct stages: (1) translocation and accumulation in plant organs; (2) translocation in vascular tissues and their interactions; and (3) association at cellular and subcellular compartments [29]. These three tiers correspond to observations at the macroscale, microscale, and molecular level, respectively. Fig. 2 shows the hierarchical structure of intact plant cell and cell wall, along with a simplified depiction of chemical compositions and functional groups of the main components in cell wall. A typical plant cell wall consists of three structurally and chemically differentiated layers from exterior to interior: the pectin-rich middle lamella, the hemicellulose-embedded primary cell wall containing cellulose microfibrils, and the lignified secondary cell wall. The cell membrane is located on the inside of the wall. For successful cellular internalization, CDs must sequentially overcome these plant-specific biological barriers, including multi-layered cell wall and plasma

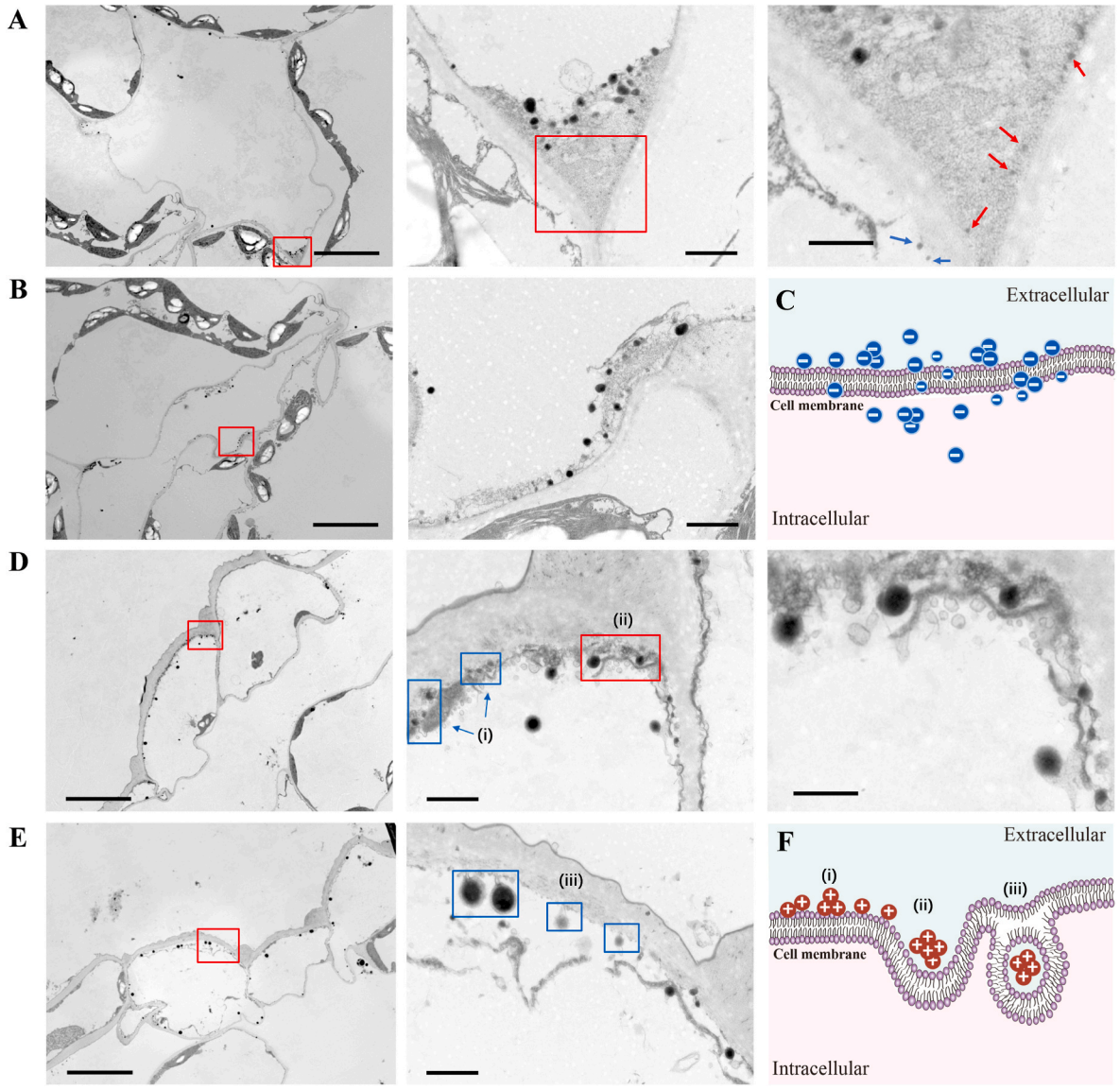

Fig. 3. TEM images localization of CDs surrounding and penetrated on the cell wall of *N. benthamiana* plants 12 h post-infiltration. (A) LCDs and (D) GCDs penetrated on the plant cell wall and localized in the intercellular space between cell wall and plasma membrane. (B) Localization of LCDs surrounding on the cell wall. (C) Proposed model for LCDs association or internalization into plant cells. (E) The GCDs-containing vesicular structures near the membrane. (F) Proposed model for GCDs association or internalization into plant cells. The red boxes from left to right indicate the areas of increased magnification. Scale bars of (A, D) from left to right, 10 μm, 1 μm, 500 nm. Scale bars of (B, E) from left to right, 10 μm, 1 μm. (For interpretation of the references to colour in this figure legend, the reader is referred to the Web version of this article.)

membrane. Abundant charged functional groups (e.g., carboxyl and hydroxyl) within plant cell wall components may impose significant hindrance to charged CDs during cellular entry process.

Intact plant leaf tissue contains two critical barriers, the wall and membrane that prevent nanoparticles from entering plant cells. To confirm and directly visualize the internalization and subcellular distribution of CDs in plant cells, we collected CDs-infiltrated *N. benthamiana* leaf tissues 12 h post-infiltration. *N. benthamiana* leaves were fixed and sectioned, and then imaged it by TEM. The absence of particulate structures in negative controls provides definitive evidence that the electron-dense entities in CDs-treated samples are exogenous CDs (Supplementary Fig. 2). Fig. 3 shows increased magnifications for LCDs and GCDs in leaves. TEM examination identified that CDs were mainly surrounding the mesophyll cell wall. The observed sizes enlargement of CDs was potentially due to aggregation induced by the plant tissue microenvironmen [42,43]. The distribution of LCDs was relatively uniform, spreading on the plant cell walls and showing a linear arrangement, indicating that they may have formed a state of stable adsorption with the cell wall (Fig. 3A and B). Cellular ultrastructure analysis revealed well-preserved cell wall integrity, suggesting that LCDs exposure did not induce significant morphological damage to cell wall structure. The aggregation of GCDs in plant tissues was more significant than that of LCDs (Fig. 3D, E and Supplementary Fig. 3). Larger aggregated particles interact with cell walls in different ways, such as exhibiting stronger adsorption or embedding into the cell wall matrix. Polysaccharides in the cell wall could interact with charged CDs through the carboxyl group. The distinct association behaviors of different charged CDs likely stem from electrostatic attraction between GCDs (+) and cell wall (−), which favors higher adhesion than that of LCDs. Similar findings in previous studies have shown that neutral QDs-MPA exhibited greater dispersion and aggregation on lateral and fibrous roots compared to negatively charged QDs-PEG-COOH [41]. Positively charged NH_2-GQDs exhibited enhanced foliar accumulation and aggregation degree, with a remarkable increase in size from 15.1 nm

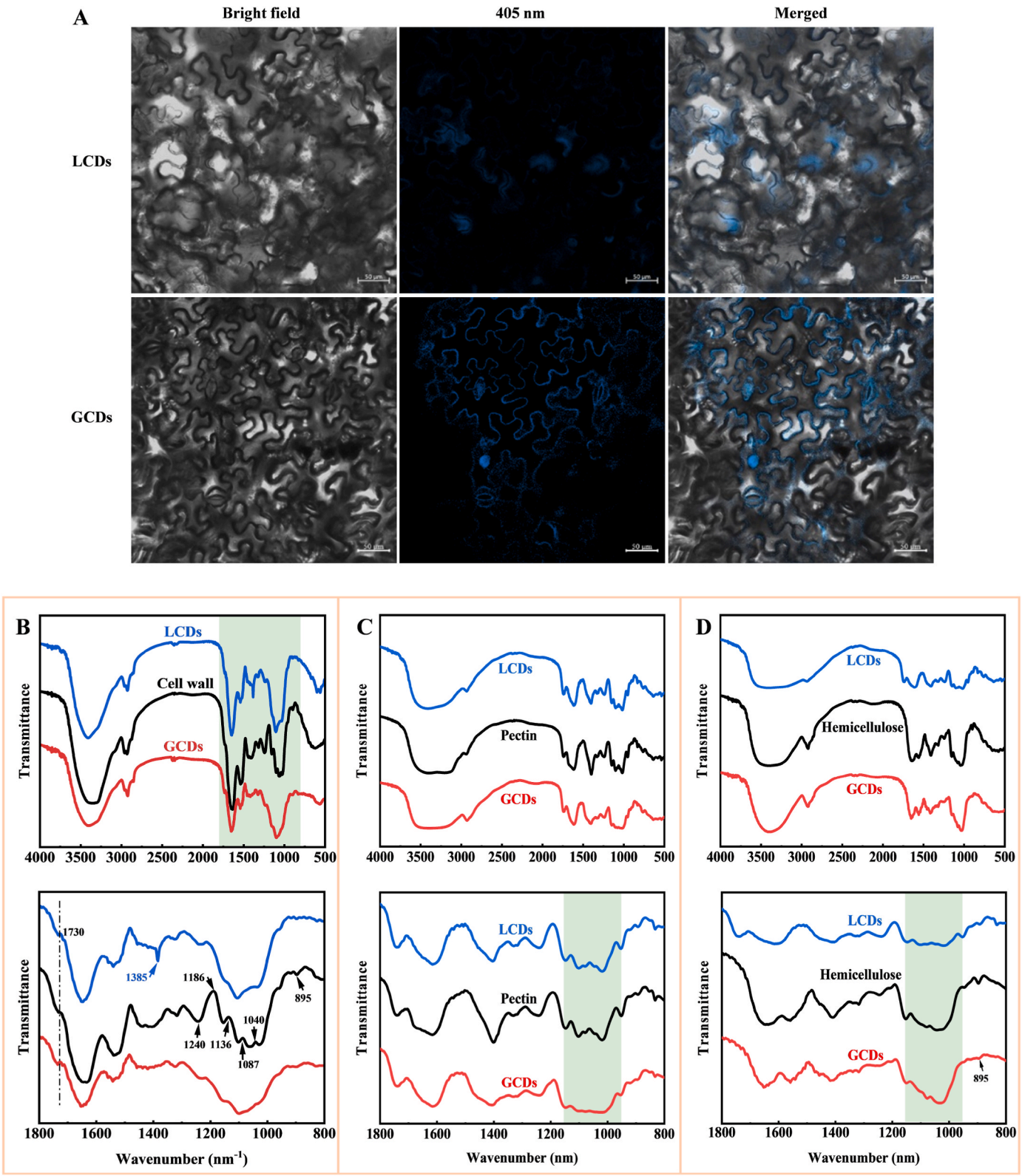

Fig. 4. Plant cell walls interact with charged CDs. (A) Representative confocal images of *N. benthamiana* leaves treated with LCDs and GCDs aqueous solution after 10 h, scale bar is 50 μm. FTIR spectra of *N. benthamiana* leaves (B) cell wall, (C) pectin and (D) hemicellulose interact with charged CDs.

to 102.8 nm, whereas negatively charged OH-GQDs showed moderate size enlargement from 13.7 nm to 74.2 nm [43]. CdSe/CdZnS QDs with positive and neutral charge exhibited particle aggregation tendencies in *Arabidopsis* leaf petioles vascular tissue and root cells, while negatively charged counterparts remained dispersed [44].

However, the phenomenon of negatively charged LCDs aggregating on negatively charged cell walls seems theoretically contradictory. Therefore, to find out why LCDs aggregate on cell walls, the pH of LCDs and GCDs dispersions have been measured. The pH of LCDs dispersions in distilled water was approximately 5.30–5.60, while GCDs has slightly

higher pH of 6.00–6.10 (Supplementary Table 1). It has been reported that the negative charge of plant cell wall is primarily contributed by pectin or glucuronoarabinoxylan (70–90 %), and the distribution of negative charges is not entirely uniform [39,45]. In particular, the cell wall network may exhibit neutral or weakly negative regions due to pectin of different degree of methyl esterification [46]. The pH of CDs affects the protonation state of certain components in the cell wall microenvironment, and thus alters the charge distribution of the cell wall. At lower pH, protonation of some carboxyl groups in the cell wall reduces the negative charge density [47,48], thereby weakening electrostatic repulsion with LCDs. Meanwhile, short-range interactions may also play a role. The LCDs may retain hydrophobic characteristics of the lignin substrate, enabling adsorption and aggregation of LCDs to hydrophobic regions of the cell wall through hydrophobic interactions. Hydroxyl groups on the surface of LCDs may also form hydrogen bonds with polar groups in the cell wall (e.g., cellulose hydroxyls) [41], overcoming partially charge repulsion and facilitating LCDs attachment near the cell wall or membrane. Additionally, although the cell wall is overall electronegative, its surface can indirectly bind negatively charged LCDs through cation bridging (e.g., Ca^{2+}, Mg^{2+}) [48,49], forming ternary complexes (pectin–COO–Ca^{2+}↔LCDs-) that promote aggregation. In Fig. 3C, we propose that LCDs association or internalization into plant cells in a relatively dispersed form. Charge repulsion enhances the dispersibility of LCDs in plants, but there are multiple mechanisms driving the adsorption and aggregation of LCDs.

Large particles in GCDs treated samples exert mechanical pressure that compromises cell wall integrity, subsequently altering wall permeability and triggering cellular response mechanisms. The aggregation of GCDs in the cell wall and their extrusion through the cell interface were observed, representing distinct stages of GCDs internalization (Fig. 3D and E). Interestingly, GCDs-containing saccular-like structures near the membrane had been found in GCDs-treated *N. benthamiana* mesophyll (Fig. 3E). In addition, ultrastructural analysis revealed multiple GCDs simultaneously encapsulated within single vesicles (Supplementary Fig. 3), suggesting that cellular internalization of positively charged CDs via membrane deformation mediated endocytosis. In contrast, no such structures were found in the leaves treated with LCDs, indicating that LCDs do not cause significant cell membrane deformation. Crucially, no GCDs-containing vesicles were observed in wortmannin-treated samples (Supplementary Fig. 4), further confirming clathrin is involved in GCDs internalization. Blue boxes in Fig. 3D and E indicate three processes of GCDs association or internalization into plant cells: (i) aggregated GCDs on the surface of the plasma membrane; (ii) aggregated large particles cause membrane invagination; (iii) plasma membrane invaginates to form vesicular structures. Thus, we summarized a model for GCDs association or internalization into plant cells (Fig. 3F). Initially, GCDs were recruited and aggregated at the cell wall, subsequently, aggregated GCDs extruded through the cell interface, ultimately leading to membrane invagination and vesicle formation. Based on these findings, we propose that there are differences in the mechanism of different charged CDs transport within plant leaf tissues. As previously reported, negatively charged PEGylated QDs had no obvious aggregation under strong ionic strength conditions in vitro and during the uptake by animal cells [50]. Therefore, we conclude that cell walls, the typical plant structure absent in animal cells, serve as a critical role in regulating CDs spatial distribution during internalization processes. Briefly, following introduction into leaves, negatively and positively charged CDs migrate toward plant cell peripheries, demonstrating pronounced association with the cell wall. Positively charged GCDs form large particles due to strong aggregation, inducing vesicle formation and then entering plant cells by the way of endocytosis, while negatively charged LCDs through non vesicular endocytosis or free diffusion due to their smaller aggregated size.

3.3. Specific distribution and interaction of charged CDs in cell wall

We explored the distribution of charged CDs in intact leaves, and subsequently conducted independent investigations into the interactions between cell walls and CDs. Charged CDs had been used to infiltrate into *N. benthamiana* leaves. The leaves uptake and distribution of CDs were determined by observing CDs fluorescence in extracellular space and mesophyll cells. CLSM imaging at 10 h post-exposure indicated that CDs of negative and positive charge penetrated through the leaf surface (Fig. 4A, Supplementary Fig. 5 and Supplementary Fig. 6). CDs signals were observed in the leaves, the fluorescence of negatively charged LCDs appeared randomly in leaf cells, while signals of positively charged GCDs regularly appeared near the cell periphery than that of LCDs. Fluorescence of GCDs was also observed in the cell and nuclear regions. The anionic characteristics of plant cell walls originate from their structural polysaccharide composition, particularly the high-density carboxyl groups in galacturonic or glucuronic acid units. Both the cell wall and membrane exhibit electronegativity, resulting in significant obstacles for negatively charged LCDs to enter the cell. The penetration time and trajectory of LCDs are inconsistent, leading to irregular distribution of fluorescence signals in intact leaves. GCDs are attracted by negatively charged cell walls and deposit more regularly around the cell wall, resulting in a stronger fluorescence signal of the cell contour profile. Previous study had shown that nanoparticles with positive charge present more accumulation in leaves [51]. Similarly, positively charged NH_2-GQDs demonstrated higher deposition (~2.1 times) on corn leaf compared to negatively charged OH-GQDs, attributed to negatively charged cell wall [43]. Another case in recent study showed more accumulation of PEI-CDs than negatively charged one at leaf surface [52]. Positive charge is crucial for the high accumulation and translocation capacity of nanoparticles to leaf cells and organelles. The weakly dissociating acidic groups, such as galacturonic acid in pectin, confer the plant cell wall a net negative charge, allowing the cell wall to behave as an ion exchanger, where the fixed cell wall charge interacts with exchangeable ions [40,48]. The chemical interactions between nanoparticles with positive charge and polysaccharide hydroxyl/carboxylate residues constitute significant determinants the intracellular transport and spatial distribution of nanoparticles in planta. According to Jeon and colleagues' work, while positively PEI-CD has a stronger binding affinity to pectin, negatively and neutrally charged CDs failed to exhibit detectable signals with pectin-based model cell walls. As a polysaccharide rich in hydroxyl groups, cellulose also interacts with PEI-CD, but their interactions displayed a much smaller extent compared to pectin counterparts [40]. The interaction between charged CDs and cell walls presents potential application in mitigating heavy metal stress. Studies have shown that the cell wall is a barrier to prevent the uptake of cationic heavy metals, and that CDs alleviate cadmium toxicity in wheat seedlings by adsorbing Cd^{2+} (reducing its bioavailability) and regulating associated gene expression [25,53,54]. This synergistic mechanism suggests that CD application may enhance protective effects in agricultural production systems.

To elucidate the function of cell wall components in mediating charged CDs uptake, cell walls of *N. benthamiana* leaves have been extracted, and then fully mixed and interacted with charged CDs. The interaction of isolated hemicellulose and pectin with CDs was also further investigated. The FTIR spectrum (Fig. 4B–D) reflects the characteristic functional groups in *N. benthamiana* leaf cell wall components. Changes occurred in the FTIR band between 1200 and 900 cm^{-1} in LCDs and GCDs treated group compared to the control (Fig. 4B). The band of 1200-900 cm^{-1} is the carbohydrate fingerprint region [55], which is very complex and dominated by ring vibrations of the C–OH side groups and the C–*O*–C glycosidic bond from polysaccharides. The peak at 895 cm^{-1} assigned to C–H bending vibrations of β-glycosidic linkage, corresponding to hemicellulose or pectin [55,56], is observed to almost disappear in both LCDs- and GCDs-cell wall interaction samples (Fig. 4B). Separate incubation experiments with charged CDs and

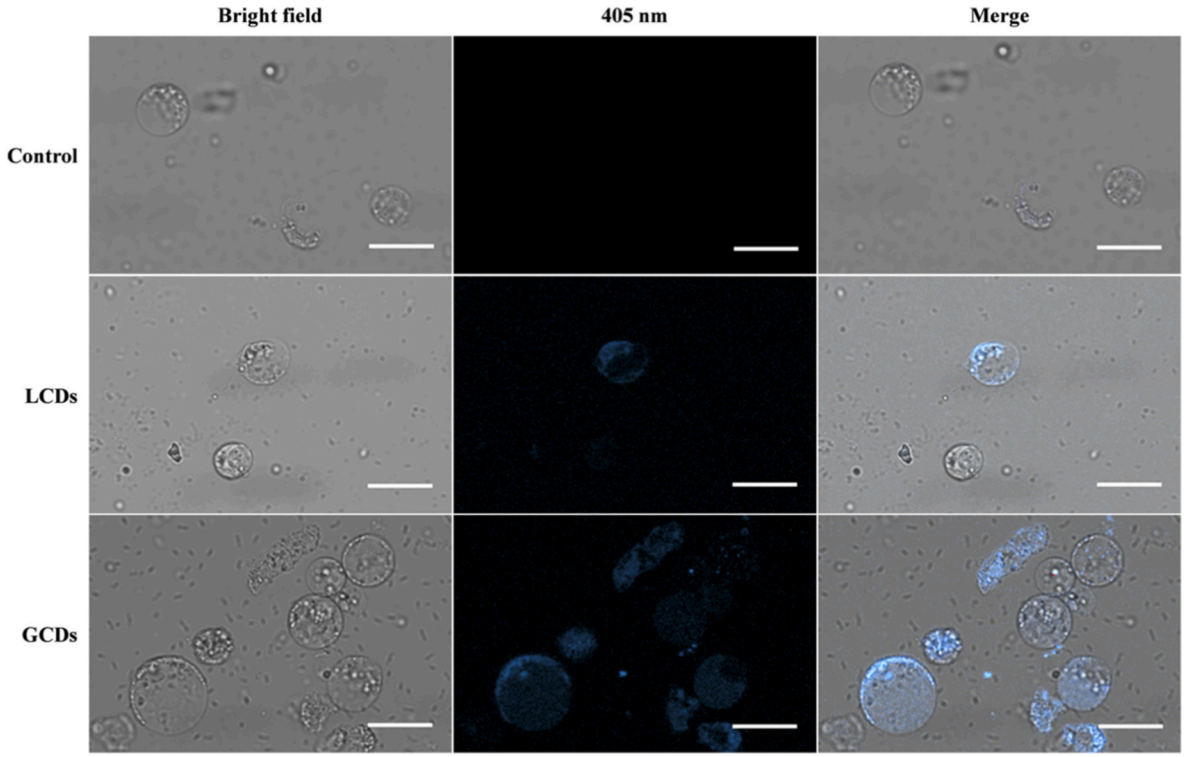

Fig. 5. The confocal images of isolated protoplasts incubated with charged CDs. Protoplasts were incubated with 0.5 mg/mL charged CDs for 2 h. Scale bar is 20 μm.

isolated hemicellulose/pectin revealed that this change was primarily attributed to hemicellulose (Fig. 4C and D). Especially, the GCDs-hemicellulose interaction led to the vigorous attenuation of the characteristic peak at 895 cm^{-1} (Fig. 4D). Peaks at 1040 and 1087 cm^{-1} are associated with sugars (e.g., arabinose, xylose, and galactose) [57]. In contrast to the control, these two peaks decrease in CDs treated group and completely disappear in GCDs treated sample. The absorbance at 1040 cm^{-1} is closely related to hemicellulose [56], while 1085 cm^{-1} is assigned to C–C stretching relating to pectin [55]. Peaks at 1150-1000 cm^{-1} are due to homogalacturonan [57], which is one of the main components in pectin. When cell wall samples were exposed to LCDs and GCDs, a sharp decrease was observed at the peaks of 1136 cm^{-1} and 1186 cm^{-1} (Fig. 4B). In the 1150-1000 cm^{-1} region (C–*O*–C/C–OH vibrations), significant band alterations occurred in pectin upon GCDs binding, contrasting with minor perturbations induced by LCDs (Fig. 4C). Conversely, hemicellulose underwent marked spectral restructuring when interacting with LCDs, while showing marginal changes to GCDs exposure (Fig. 4D). Peak around 1136 cm^{-1} corresponds specifically to vibrations of glycosidic C–*O*–C linkages [57]. C–O stretching of polysaccharides at 1186 cm^{-1} can be observed in hemicellulose and lignin isolated from poplar [56]. The peak of 1186 cm^{-1} in lignin related to the small portion of lignin-carbohydrate resistance linkage retained during lignin extraction [56,58]. Peaks in range of 1750-1200 cm^{-1} in the FTIR spectrum of plant cell wall might relate to the characteristic signals of lignin and lignin crosslinked polysaccharides. In *N. benthamiana* leave cell wall material, C–H_2 bending at 1385 cm^{-1} corresponding to hemicellulose [56] appeared in LCDs group (Fig. 4B), while this peak appeared in GCDs group in the cell wall of rice (Supplementary Fig. 7). There are significant differences in the types of hemicellulose monosaccharide polymerization contained in different plants [59], which may affect the interaction between CDs and cell walls. The peaks at 1730 cm^{-1} (C═O vibration) and 1240 cm^{-1} (C–O stretching) are attributed to acetyl groups (O═C–H) and carboxyl group (O═C–O) [60]. These characteristic peaks represent acetyl groups connected with ester bonds in hemicellulose or the aldehyde ester groups in hemicellulose-lignin complex. It can be seen a slight change at 1730 cm^{-1} and a significant variation at 1240 cm^{-1}, suggesting the interaction between the cell wall and CDs might also occur in hydrophobic domains. In summary, two different surface charge CDs changed the intensity of certain functional groups. These findings emphasize that the interaction between charged CDs and cell walls is mainly dominated by polysaccharides, particularly hemicellulose and pectin fractions, including lignin-cross-linked-polysaccharides.

3.4. *Membrane affinity of charged CDs in isolated protoplasts*

Previous studies have overlooked the dynamic interconnections between plant-specific hierarchical barriers, leading to a fragmented understanding of nanoparticle entry into plant cells. Following analysis of CDs-cell wall interactions, plant protoplasts were prepared by cell wall removal to further examine the effects of the cell membrane on nanoparticle entry into cells. We incubated the protoplasts with charged CDs (0.5 mg/mL) in darkness for 2 h and then observed them under a laser confocal microscope. The photoluminescence properties of carbon dots make them traceable for interaction with plant tissues and cells. We found that compared with negatively charged LCDs, positively charged GCDs were more easily assimilated by the protoplasts of *Oryza sativa* L. (Fig. 5). Plant plasma membrane is highly electronegative according to Simon and colleagues' study [61]. Membrane electrostatics largely depends on anionic phospholipids, like phosphatidylserine [7]. Strong negative surface charge of the plasma membrane may be sufficient to specifically target positively charged polycationic proteins [62]. Thus, GCDs demonstrate enhanced binding affinity toward protoplasts, driven by electrostatic interactions with the anionic membrane surface.

The mechanism driving the interaction between negatively charged nanomaterials and cell membranes remains unclear, but could involve transient modifications (e.g., dynamic adsorption of biomolecules or corona formation) that induce enhanced positive charge and promote membrane interaction [63]. In a study of cucumber and *Arabidopsis*, protoplasts had better uptake on CDs with negative charge compared to positively charged CDs [52]. The uptake and distribution of AuNPs with different functional groups were correlated with both the surface charge

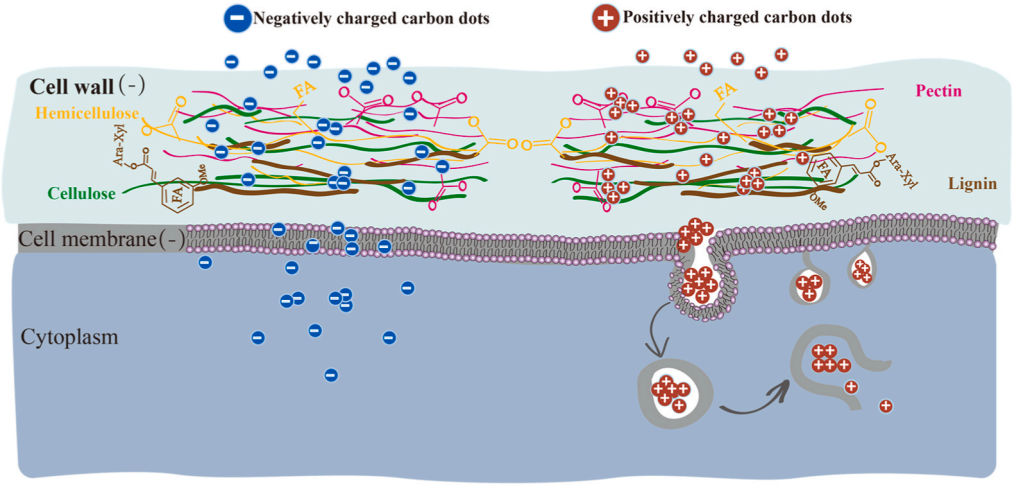

Fig. 6. Mechanistic schematic for charged CDs association or internalization into plant cells. "FA" represents esterification with ferulic acid, which is characteristic of hemicellulose polysaccharides.

of the nanoparticles and the plant species [39]. In this work, the protoplasts of the monocotyledonous plant *Oryza sativa* L. were co-incubated with charged CDs, while the protoplasts of the dicotyledonous plants cucumber and *Arabidopsis* had been used in previous study. In another study, SWNTs with high zeta potential, whether it is positively or negatively charged, were effectively delivered into *Arabidopsis* protoplasts [18]. This indicates that the uptake of nanoparticles by protoplasts may be related not only to the shape and surface charge, but also to differences in plant species and classification.

3.5. Transport mechanisms of charged CDs in plant cells

As previously stated, extant researches have predominantly neglected the spatiotemporal coordination of plant-specific multi-layered barriers, engendering reductionist interpretations of nanoparticles translocation mechanisms. We employed multi-scale and multi-dimensional approaches to investigate the continuum of CDs internalization trajectories and correlation, thereby enhancing the systematic comprehension of nanoparticles behavior in plant systems.

Integrating experimental evidence, we propose a translocation model for charged CDs transport into plant cells (Fig. 6). During the initial introducing mature plant leaves, charged CDs transport around plant cells. The presence of carboxyl groups and other negatively charged groups in pectin and hemicellulose polysaccharides contribute to an overall negative charge within the cell wall. Electrostatic interactions cause positively charged CDs easily bind with pectin and hemicellulose in the cell wall, leading to aggregation. The CDs with negative charge are repelled by the electronegativity of the cell wall, reducing the likelihood of aggregation. Meanwhile, the components of plant cell walls exhibit heterogeneous temporal and spatial distributions, leading to non-uniform charge distribution that causes varying degrees of aggregation among charged LCDs. Positively charged CDs are strongly adsorbed by the cell wall and accumulate on the surface of the cell wall to form a high concentration area, which exerts pressure. Meanwhile, the reaction between positively charged CDs and cell wall components may alter the flexibility and permeability of the cell wall. These factors enable positively charged CDs that aggregate into larger particles to overcome the barriers and limitations imposed by the cell wall. After passing through the cell wall, positively charged CDs are electrostatic adsorbed with negatively charged cell membranes and aggregate on the surface. The aggregation of positively charged CDs on the membrane surface exerts local pressure, resulting in membrane deformation. During this process, the cell membrane invaginates and envelops the positively charged CDs, forming vesicles that are subsequently transported into the cell.

4. Conclusion

Plant cellular barriers possess unique characteristics as a multi-layered barrier system. We designed and synthesized biomass-derived CDs with different surface charges for assessing and simulating charge-dependent interfacial interaction. Real-time fluorescence confocal microscopy revealed charge-correlated distribution in protoplasts and mesophyll cells, with preferential accumulation of positively charged CDs at cell walls. Hemicellulose and pectin dominated interaction between charged CDs and cell walls, while positively charged CDs exhibited a higher affinity for negatively charged membranes and walls. In addition, positively charged CDs induced membrane interfacial remodeling, triggering localized aggregation at membrane-wall junctions. This promoted membrane invagination and vesicle-mediated internalization, contrasting with permeation of negatively charged counterparts. These findings demonstrate charge-specific internalization mechanisms: positive charges facilitate active membrane remodeling, whereas negative charges rely on physicochemical compatibility. These insights elucidate how nanoscale surface properties dictate plant cell interface dynamics, providing a framework for rational design of phytonanotechnology systems.

CRediT authorship contribution statement

Luyao Wei: Writing – original draft, Methodology, Investigation, Data curation, Conceptualization. **Binshou Wang:** Investigation, Data curation. **Shuling Cao:** Investigation, Data curation. **Hang Tan:** Investigation, Data curation. **Tianyi Long:** Data curation. **Chuanfei Bian:** Data curation. **Liangcai Peng:** Writing – review & editing. **Hongliang Wang:** Writing – review & editing, Supervision, Funding acquisition, Conceptualization. **Xu Cheng:** Writing – review & editing. **Wanbin Zhu:** Writing – review & editing, Supervision, Funding acquisition, Conceptualization.

Declaration of competing interest

The authors declare that they have no known competing financial interests or personal relationships that could have appeared to influence the work reported in this paper.

Acknowledgments

This work was supported by the Project of Sanya Yazhou Bay Science and Technology City (SCKJ-JYRC-2022-51), the Beijing Innovation Team of the Modern Agricultural Industrial Technology System (BAIC08-2023-FQ02), the National Key Research and Development Program of China (2023YFD1701504), National Natural Science Foundation of China (22278422), and the 2115 Talent Development Program of China Agricultural University Fund (1011–00109018).

Appendix A. Supplementary data

Supplementary data to this article can be found online at https://doi.org/10.1016/j.carbon.2025.120747.

References

[1] W. Elmer, J.C. White, The future of nanotechnology in plant pathology, Annu. Rev. Phytopathol. 56 (2018) 111–133, https://doi.org/10.1146/annurev-phyto-080417-050108.
[2] G.V. Lowry, A. Avellan, L.M. Gilbertson, Opportunities and challenges for nanotechnology in the agri-tech revolution, Nat. Nanotechnol. 14 (6) (2019) 517–522, https://doi.org/10.1038/s41565-019-0461-7.
[3] G.S. Demirer, H. Zhang, N.S. Goh, E. González-Grandío, M.P. Landry, Carbon nanotube–mediated DNA delivery without transgene integration in intact plants, Nat. Protoc. 14 (10) (2019) 2954–2971, https://doi.org/10.1038/s41596-019-0208-9.
[4] F.J. Cunningham, N.S. Goh, G.S. Demirer, J.L. Matos, M.P. Landry, Nanoparticle-mediated delivery towards advancing plant genetic engineering, Trends Biotechnol. 36 (9) (2018) 882–897, https://doi.org/10.1016/j.tibtech.2018.03.009.
[5] J.W. Wang, E.G. Grandio, G.M. Newkirk, G.S. Demirer, S. Butrus, J.P. Giraldo, et al., Nanoparticle-mediated genetic engineering of plants, Mol. Plant 12 (8) (2019) 1037–1040, https://doi.org/10.1016/j.molp.2019.06.010.
[6] Q. Zhang, Y. Ying, J. Ping, Recent advances in plant nanoscience, Adv. Sci. 9 (2) (2021), https://doi.org/10.1002/advs.202103414.
[7] J. Bigay, B. Antonny, Curvature, lipid packing, and electrostatics of membrane organelles: defining cellular territories in determining specificity, Dev. Cell 23 (5) (2012) 886–895, https://doi.org/10.1016/j.devcel.2012.10.009.
[8] M.P. Landry, N. Mitter, How nanocarriers delivering cargos in plants can change the GMO landscape, Nat. Nanotechnol. 14 (6) (2019) 512–514, https://doi.org/10.1038/s41565-019-0463-5.
[9] T.T.S. Lew, R. Sarojam, I.C. Jang, B.S. Park, N.I. Naqvi, M.H. Wong, et al., Species-independent analytical tools for next-generation agriculture, Nat. Plants 6 (12) (2020) 1408–1417, https://doi.org/10.1038/s41477-020-00808-7.
[10] L. Wei, J. Liu, G. Jiang, Nanoparticle-specific transformations dictate nanoparticle effects associated with plants and implications for nanotechnology use in agriculture, Nat. Commun. 15 (1) (2024), https://doi.org/10.1038/s41467-024-51741-8.
[11] J. Hong, J.R. Peralta-Videa, C. Rico, S. Sahi, M.N. Viveros, J. Bartonjo, et al., Evidence of Translocation and physiological impacts of foliar applied CeO_2 nanoparticles on cucumber (*Cucumis sativus*) plants, Environ. Sci. Technol. 48 (8) (2014) 4376–4385, https://doi.org/10.1021/es404931g.
[12] J.S. Park, W. Park, S.j. Park, A.C. Larson, D.H. Kim, K.H. Park, Multimodal magnetic nanoclusters for gene delivery, directed migration, and tracking of stem cells, Adv. Funct. Mater. 27 (25) (2017), https://doi.org/10.1002/adfm.201700396.
[13] G. Griffiths, J. Gruenberg, M. Marsh, J. Wohlmann, A.T. Jones, R.G. Parton, Nanoparticle entry into cells; the cell biology weak link, Adv. Drug Deliv. Rev. 188 (2022) 114403, https://doi.org/10.1016/j.addr.2022.114403.
[14] E. Navarro, A. Baun, R. Behra, N.B. Hartmann, J. Filser, A.J. Miao, et al., Environmental behavior and ecotoxicity of engineered nanoparticles to algae, plants, and fungi, Ecotoxicology 17 (5) (2008) 372–386, https://doi.org/10.1007/s10646-008-0214-0.
[15] J.D. Hubbard, A. Lui, M.P. Landry, Multiscale and multidisciplinary approach to understanding nanoparticle transport in plants, Curr. Opin. Chem. Eng. 30 (2020) 135–143, https://doi.org/10.1016/j.coche.2020.100659.
[16] C. Rondeau-Mouro, D. Defer, E. Leboeuf, M. Lahaye, Assessment of cell wall porosity in Arabidopsis thaliana by NMR spectroscopy, Int. J. Biol. Macromol. 42 (2) (2008) 83–92, https://doi.org/10.1016/j.ijbiomac.2007.09.020.
[17] H. Wu, Z. Li, Nano-enabled agriculture: how do nanoparticles cross barriers in plants? Plant Commun 3 (6) (2022) https://doi.org/10.1016/j.xplc.2022.100346.
[18] T.T.S. Lew, M.H. Wong, S.Y. Kwak, R. Sinclair, V.B. Koman, M.S. Strano, Rational design principles for the transport and subcellular distribution of nanomaterials into plant protoplasts, Small 14 (44) (2018) e1802086, https://doi.org/10.1002/smll.201802086.
[19] E.A.K. Warren, C.K. Payne, Cellular binding of nanoparticles disrupts the membrane potential, RSC Adv. 5 (18) (2015) 13660–13666, https://doi.org/10.1039/c4ra15727c.
[20] H. Wu, L. Shabala, S. Shabala, J.P. Giraldo, Hydroxyl radical scavenging by cerium oxide nanoparticles improves Arabidopsis salinity tolerance by enhancing leaf mesophyll potassium retention, Environ. Sci. Nano 5 (7) (2018) 1567–1583, https://doi.org/10.1039/c8en00323h.
[21] M.H. Wong, R.P. Misra, J.P. Giraldo, S.Y. Kwak, Y. Son, M.P. Landry, et al., Lipid exchange envelope penetration (LEEP) of nanoparticles for plant engineering: a universal localization mechanism, Nano Lett. 16 (2) (2016) 1161–1172, https://doi.org/10.1021/acs.nanolett.5b04467.
[22] W. Li, Y. Zheng, H. Zhang, Z. Liu, W. Su, S. Chen, et al., Phytotoxicity, uptake, and translocation of fluorescent carbon dots in mung bean plants, ACS Appl. Mater. Interfaces 8 (31) (2016) 19939–19945, https://doi.org/10.1021/acsami.6b07268.
[23] C. Xia, S. Zhu, T. Feng, M. Yang, B. Yang, Evolution and synthesis of carbon dots: from carbon dots to carbonized polymer dots, Adv. Sci. 6 (23) (2019) 1901316, https://doi.org/10.1002/advs.201901316.
[24] H. Yu, G. Zhang, J. Liu, P. Liu, H. Peng, Z. Teng, et al., A functional cascading of lignin modification via repression of caffeic acid O-methyltransferase for bioproduction and anti-oxidation in rice, J. Adv. Res. (2025), https://doi.org/10.1016/j.jare.2025.01.048.
[25] L. Xiao, H. Guo, S. Wang, J. Li, Y. Wang, B. Xing, Carbon dots alleviate the toxicity of cadmium ions (Cd^{2+}) toward wheat seedlings, Environ. Sci. Nano 6 (5) (2019) 1493–1506, https://doi.org/10.1039/c9en00235a.
[26] C. Zhao, X. Wang, L. Yu, L. Wu, X. Hao, Q. Liu, et al., Quaternized carbon quantum dots with broad-spectrum antibacterial activity for the treatment of wounds infected with mixed bacteria, Acta Biomater. 138 (2022) 528–544, https://doi.org/10.1016/j.actbio.2021.11.010.
[27] R. Wang, G. Xia, W. Zhong, L. Chen, L. Chen, Y. Wang, et al., Direct transformation of lignin into fluorescence-switchable graphene quantum dots and their application in ultrasensitive profiling of a physiological oxidant, Green Chem. 21 (12) (2019) 3343–3352, https://doi.org/10.1039/c9gc01012b.
[28] Y. Zhang, J. Su, S. Duan, Y. Ao, J. Dai, J. Liu, et al., A highly efficient rice green tissue protoplast system for transient gene expression and studying light/chloroplast-related processes, Plant Methods 7 (2011) 30.
[29] H. Zhang, N.S. Goh, J.W. Wang, R.L. Pinals, E. Gonzalez-Grandio, G.S. Demirer, et al., Nanoparticle cellular internalization is not required for RNA delivery to mature plant leaves, Nat. Nanotechnol. 17 (2) (2022) 197–205, https://doi.org/10.1038/s41565-021-01018-8.
[30] D.C. Elias, R.R. Nair, T.M.G. Mohiuddin, S.V. Morozov, P. Blake, M.P. Halsall, et al., Control of graphene's properties by reversible hydrogenation evidence for graphane, Science 323 (5914) (2009) 610–613, https://doi.org/10.1126/science.1167130.
[31] H. Xu, J. Chang, H. Wu, H. Wang, W. Xie, Y. Li, et al., Carbon dots with guanidinium and amino acid functional groups for targeted small interfering RNA delivery toward tumor gene therapy, Small 19 (31) (2023) e2207204, https://doi.org/10.1002/smll.202207204.
[32] A. Kundu, S. Nandi, P. Das, A.K. Nandi, Facile and green approach to prepare fluorescent carbon dots: emergent nanomaterial for cell imaging and detection of vitamin B2, J. Colloid Interface Sci. 468 (2016) 276–283, https://doi.org/10.1016/j.jcis.2016.01.070.
[33] M. Hasani, H.R. Kalhor, Enzyme-inspired lysine-modified carbon quantum dots performing carbonylation using urea and a cascade reaction for synthesizing 2-benzoxazolinone, ACS Catal. 11 (17) (2021) 10778–10788, https://doi.org/10.1021/acscatal.1c01276.
[34] Z. Ding, F. Li, J. Wen, X. Wang, R. Sun, Gram-scale synthesis of single-crystalline graphene quantum dots derived from lignin biomass, Green Chem. 20 (6) (2018) 1383–1390, https://doi.org/10.1039/c7gc03218h.
[35] F.-F. Tan, X.-Y. He, W.-F. Tian, Y. Li, Visible-light photoredox-catalyzed C–O bond cleavage of diaryl ethers by acridinium photocatalysts at room temperature, Nat. Commun. 11 (1) (2020), https://doi.org/10.1038/s41467-020-19944-x.
[36] L.-F. Zhai, M.-F. Duan, H.-Y. Guo, F. Zhang, M. Sun, Selective cleavage of C–O bond in diaryl ether contaminants via anodic oxidation, ACS Sustainable Chem. Eng. 7 (22) (2019) 18414–18420, https://doi.org/10.1021/acssuschemeng.9b04133.
[37] A. Avellan, J. Yun, Y. Zhang, E. Spielman-Sun, J.M. Unrine, J. Thieme, et al., Nanoparticle size and coating chemistry control foliar uptake pathways, translocation, and leaf-to-rhizosphere transport in wheat, ACS Nano 13 (5) (2019) 5291–5305, https://doi.org/10.1021/acsnano.8b09781.
[38] S.J. Jeon, Y. Zhang, C. Castillo, V. Nava, K. Ristroph, B. Therrien, et al., Targeted delivery of sucrose-coated nanocarriers with chemical cargoes to the plant vasculature enhances long-distance translocation, Small 20 (7) (2024) e2304588, https://doi.org/10.1002/smll.202304588.
[39] Z.J. Zhu, H. Wang, B. Yan, H. Zheng, Y. Jiang, O.R. Miranda, et al., Effect of surface charge on the uptake and distribution of gold nanoparticles in four plant species, Environ. Sci. Technol. 46 (22) (2012) 12391–12398, https://doi.org/10.1021/es301977w.
[40] S.J. Jeon, P. Hu, K. Kim, C.M. Anastasia, H.-I. Kim, C. Castillo, et al., Electrostatics control nanoparticle interactions with model and native cell walls of plants and algae, Environ. Sci. Technol. 57 (48) (2023) 19663–19677, https://doi.org/10.1021/acs.est.3c05686.
[41] H. Sun, M. Wang, C. Lei, R. Li, Cell wall: an important medium regulating the aggregation of quantum dots in maize (*Zea mays L.*) seedlings, J. Hazard. Mater. 403 (2021), https://doi.org/10.1016/j.jhazmat.2020.123960.
[42] S. Lin, J. Reppert, Q. Hu, J.S. Hudson, M.L. Reid, T.A. Ratnikova, et al., Uptake translocation and transmission of carbon nanomaterials in rice plants, Small 5 (10) (2009) 1128–1132, https://doi.org/10.1002/smll.200801556.
[43] H. Sun, M. Wang, J. Wang, W. Wang, Surface charge affects foliar uptake, transport and physiological effects of functionalized graphene quantum dots in plants, Sci. Total Environ. 812 (2022), https://doi.org/10.1016/j.scitotenv.2021.151506.
[44] Y. Koo, J. Wang, Q. Zhang, H. Zhu, E.W. Chehab, V.L. Colvin, et al., Fluorescence reports intact quantum dot uptake into roots and translocation to leaves of

Arabidopsis thaliana and subsequent ingestion by insect herbivores, Environ. Sci. Technol. 49 (1) (2014) 626–632, https://doi.org/10.1021/es5050562.
[45] J.B. Wehr, F.P.C. Blamey, N.W. Menzies, Comparison between methods using copper, lanthanum, and colorimetry for the determination of the cation exchange capacity of plant cell Walls, J. Agric. Food Chem. 58 (8) (2010) 4554–4559, https://doi.org/10.1021/jf100097k.
[46] I. Obomighie, I.J. Prentice, P. Lewin-Jones, F. Bachtiger, N. Ramsay, C. Kishi-Itakura, et al., Understanding pectin cross-linking in plant cell walls, Commun. Biol. 8 (1) (2025), https://doi.org/10.1038/s42003-025-07495-0.
[47] N.R. Meychik, I.P. Yermakov, Ion exchange properties of plant root cell walls, Plant Soil 234 (2001) 181–193.
[48] I. Shomer, A.J. Novacky, S.M. Pike, U. Yermiyahu, T.B. Kinraide, Electrical potentials of plant cell walls in response to the ionic environment, Plant Physiol. 133 (1) (2003) 411–422, https://doi.org/10.1104/pp.103.024539.
[49] D.J. Cosgrove, Structure and growth of plant cell walls, Nat. Rev. Mol. Cell Biol. 25 (5) (2023) 340–358, https://doi.org/10.1038/s41580-023-00691-y.
[50] M. Zhang, B.P. Bishop, N.L. Thompson, K. Hildahl, B. Dang, O. Mironchuk, et al., Quantum dot cellular uptake and toxicity in the developing brain: implications for use as imaging probes, Nanoscale Adv. 1 (9) (2019) 3424–3442, https://doi.org/10.1039/c9na00334g.
[51] P. Hu, J. An, M.M. Faulkner, H. Wu, Z. Li, X. Tian, et al., Nanoparticle charge and size control foliar delivery efficiency to plant cells and organelles, ACS Nano 14 (7) (2020) 7970–7986, https://doi.org/10.1021/acsnano.9b09178.
[52] L. Zhu, W. Xu, X. Yao, L. Chen, G. Li, J. Gu, et al., Cell wall pectin content refers to favored delivery of negatively charged carbon dots in leaf cells, ACS Nano 17 (23) (2023) 23442–23454, https://doi.org/10.1021/acsnano.3c05182.
[53] J. Xin, B. Huang, J. Yang, Z. Yang, J. Yuan, Y. Mu, Role of roots in cadmium accumulation of two water spinach cultivars: reciprocal grafting and histochemical experiments, Plant Soil 366 (1–2) (2012) 425–432, https://doi.org/10.1007/s11104-012-1439-5.
[54] B. Huang, Q. Liao, H. Fu, Z. Ye, Y. Mao, J. Luo, et al., Effect of potassium intake on cadmium transporters and root cell wall biosynthesis in sweet potato, Ecotoxicol. Environ. Saf. 250 (2023) 114501, https://doi.org/10.1016/j.ecoenv.2023.114501.
[55] C. Cao, Z. Yang, L. Han, X. Jiang, G. Ji, Study on in situ analysis of cellulose, hemicelluloses and lignin distribution linked to tissue structure of crop stalk internodal transverse section based on FTIR microspectroscopic imaging, Cellulose 22 (1) (2014) 139–149, https://doi.org/10.1007/s10570-014-0525-7.
[56] S. Bhagia, J. Ďurkovič, R. Lagaňa, M. Kardošová, F. Kačík, A. Cernescu, et al., Nanoscale FTIR and mechanical mapping of plant cell walls for understanding biomass deconstruction, ACS Sustainable Chem. Eng. 10 (9) (2022) 3016–3026, https://doi.org/10.1021/acssuschemeng.1c08163.
[57] E.E. Santos, R.C. Amaro, C.C.C. Bustamante, M.H.A. Guerra, L.C. Soares, R.E. S. Froes, Extraction of pectin from agroindustrial residue with an ecofriendly solvent: use of FTIR and chemometrics to differentiate pectins according to degree of methyl esterification, Food Hydrocoll. 107 (2020), https://doi.org/10.1016/j.foodhyd.2020.105921.
[58] S. Bhagia, A.J. Ragauskas, Preserving aryl ether linkages and higher yields of isolated lignin through biomass fibrillation, ACS Sustainable Chem. Eng. 8 (1) (2020) 34–37, https://doi.org/10.1021/acssuschemeng.9b06390.
[59] H.V. Scheller, P. Ulvskov, Hemicelluloses, Annu. Rev. Plant Biol. 61 (1) (2010) 263–289, https://doi.org/10.1146/annurev-arplant-042809-112315.
[60] J. Zhu, H. Wang, F. Guo, L. Salmén, Y. Yu, Cell wall polymer distribution in bamboo visualized with in situ imaging FTIR, Carbohydr. Polym. 274 (2021), https://doi.org/10.1016/j.carbpol.2021.118653.
[61] M.L. Simon, M.P. Platre, M.M. Marques-Bueno, L. Armengot, T. Stanislas, V. Bayle, et al., A PtdIns(4)P-driven electrostatic field controls cell membrane identity and signalling in plants, Nat. Plants 2 (2016) 16089, https://doi.org/10.1038/nplants.2016.89.
[62] G. Molnar, M. Fendrych, J. Friml, Plasma membrane: negative attraction, Nat. Plants 2 (7) (2016) 16102, https://doi.org/10.1038/nplants.2016.102.
[63] A. Wang, Q. Jin, X. Xu, A. Miao, J.C. White, J.L. Gardea-Torresdey, et al., High-throughput screening for engineered nanoparticles that enhance photosynthesis using mesophyll protoplasts, J. Agric. Food Chem. 68 (11) (2020) 3382–3389, https://doi.org/10.1021/acs.jafc.9b06429.